Robust control scheme based on an uncertainty and disturbance estimator for a quadrotor with motor failures

Julio Betancourt, Vicente Balaguer, Pedro Castillo Garcia, Pedro García, Rogelio Lozano

Robust control scheme based on an uncertainty and disturbance estimator for a quadrotor with motor failures

Julio Betancourt *
Sorbonne Universités, Université de Technologie de Compiègne,
CNRS, Heudiasyc UMR 7253, Compiègne, 60200, France
gjc.betancourt@gmail.com

Vicente Balaguer
Instituto de Automática e Informática Industrial
Universitat Politècnica de València (UPV)
vibagar3@upvnet.upv.es

Pedro Castillo
Sorbonne Universités, Université de
Technologie de Compiègne, CNRS, Heudiasyc
UMR 7253, Compiègne, 60200, France
castillo@hds.utc.fr

Pedro García
Instituto de Automática e Informática Industrial
Universitat Politècnica de València (UPV)
pggil@isa.upv.es

Rogelio Lozano
Sorbonne Universités, Université de
Technologie de Compiègne, CNRS, Heudiasyc
UMR 7253, Compiègne, 60200, France
rlozano@hds.utc.fr

Abstract

This paper proposes a new robust fault tolerant control architecture based on a disturbance observer. The control architecture is composed by a nominal controller and a rotor's fault observer capable to identify and estimate motors' degradation performance. Besides, is designed for a quadrotor vehicle and validated in critical and non critical motors' failures. For both failure cases, each motor performance is analyzed to counteracted the failure and restore the system stability. If the practical stability is not recovered (critical case) a control reconfiguration is performed for safe landing. Experimental tests are carried out in real time to illustrate the effectiveness of the proposed architecture when confronting the stability of the system with aggressive disturbances or uncertainties.

1 Introduction

Aerial quadrotor is a type of Unmanned Aerial Vehicle (UAV) which is composed by four motors and by an embedded electronic-control system where the control algorithm is executed (Zulu and John, 2016). Applications of quadrotors have focused the attention of a large part of the scientific community with respect to other UAVs configurations due to the low cost, simplicity and versatility (Amin et al., 2016), (Kerr et al., 2020), (Menouar et al., 2017). However, quadrotors have some disadvantages, they are an underactuated and unstable systems with nonlinearities, fast dynamics and couplings between its different states. This type of

*Corresponding author

aerial vehicle still represents a challenge for the control scientific community due to its different applications (Poultney et al., 2018; Saeed et al., 2015). Several control approaches were proposed in the literature for quadrotors. Most works propose solutions for challenges related with the stability and trajectory tracking. Linear controllers (as the PID and the Linear Quadratic Regulator) are the most widely used techniques in the industry and academia (Balaguer et al., 2021; Miranda-Colorado and Aguilar, 2019; Bouabdallah et al., 2004a; Outeiro et al., 2021). The main advantages of linear controllers are the simplicity to implement and tune, for achieving an acceptable performance in real time. However, its performance is degraded considerably when working outside the linear zone such as aggressive flight maneuvers (Comert, Ceren and Kasnakoglu, 2017). Hence, the application of this type of techniques is limited when dealing with real life scenarios.

One of the main problems for commercial quadrotor aerial vehicles is that their inner control architecture is not conceived for compensating rotors failures. Therefore, the failures influence the dynamics of the vehicle affecting the stability, reliability, and safety during the flight envelope. This problem makes the aerial vehicles not safe for their use on civil applications (or in populated areas). If non conventional maneuvers are required, more advanced control strategies must be considered. Strategies such as Sliding Mode Control (SMC) (Silva and Santos, 2020), H_∞ (Ortiz et al., 2016), Model Predictive Control (MPC) (Betancourt-Vera et al., 2018; Cavanini et al., 2021), BackStepping (Jia et al., 2017) or heuristic controllers (Gu et al., 2020) are examples of these types of controllers, which have been used to face aggressive behaviors. Likewise, controllers using quaternion (Abaunza and Castillo, 2019; Castillo et al., 2019) have been used to deal with these conditions. In this case, the orientation of the vehicle is described alternately to the Euler angles, which allows avoiding various problems such as the indetermination that arises with the Euler angles when encountering singularities (Castillo et al., 2016). However, the main disadvantage of some nonlinear techniques is their complexity, for executing the algorithm in real time on the vehicle and for obtaining the controller parameters. Therefore, simple controllers are preferred by non-experts users or practitioners, and some researchers have improved this kind of controllers by adding blocks/modules in the control structure, turning it into a robust control scheme.

Observer schemes, such as the Disturbance Observer Based Control (DOBC) techniques (Chen et al., 2015), are popular for non conventional tasks. They allow to increase robustness into the system against uncertainties, without a significant increase in the algorithm complexity. These techniques are based on observing the inputs and the outputs of the plant and based on the theoretical response that should be obtained attributing everything inexplicable to a disturbance (Guo and Cao, 2014). The previous results, in an equivalent disturbance that explains all the unknown behavior that can range from external disturbance to modeling errors and nonlinearities. In addition, the source of the disturbance is not relevant for these methodologies. Among the most used DOBC techniques are the Disturbance Observers (DOBs) based on input–output models (Sariyildiz et al., 2019); Active Disturbance Rejection Control (ADRC) (Han, 2009), which approximates the plant to an integrator chain and all the other behaviors are considered as disturbances; Generalized Extended State Observer (GESO) (Li et al., 2011), which uses an observer with the model and assumes that the disturbance is constant, and the Uncertainty and Disturbance Observer (UDE) (Zhong and Rees, 2004), which uses the model and the known plant state to obtain an approximation of the disturbance. This last one demonstrated its practical validation for compensating external disturbances in quadrotors (Sanz et al., 2016; Qian and Liu, 2019; Lu et al., 2020; Betancourt-Vera et al., 2020; Dhadekar et al., 2021).

For dealing with undesired and inner nonlinear performances into the system (some of them produced by actuators failures) the Fault Tolerant Control (FTC) techniques (Yin et al., 2016) are used frequently. These methods are used to deal with failures that could arise from the system, preventing the performance degradation and making the control system safe and reliable. These techniques can be classified into passive and active (Ortiz-Torres et al., 2020a). In the first case, the controller works itself to minimize the effect of the failures but it is not capable to overcome them. Nevertheless, in the second case, when the fault occurs, a self-reconfigurable controller is applied to maintain the desired performance of the system. These kinds of techniques generally use the following methodology (Zhang and Jiang, 2008; Safaeipour et al., 2021): the identification of the plant in regular operation, control tuning for the regular operation, detection and

identification of the possible fault, and the control law reconfiguration. For instance, in (Sadeghzadeh et al., 2012), the authors proposed an active FTC based on a Gain-Secheudeld PID combined with an observer capable to detect and identify faults on a quadrotor. A passive FTC was proposed in (Yu et al., 2019; Gracia et al., 2018) using a Sliding Mode Control (SMC) combined with a heuristic controller that was optimized for different possible faults scenarios, and (Lyu et al., 2017) an extra sensor observer for thrust fault was presented. A robust adaptive FTC for uncertain MIMO process system exposed to actuator faults was implemented in (Arıcı and Kara, 2020). The scheme is composed by centralized model reference adaptive control with output feedback framework for output tracking despite the presence of actuator fault regardless of time and duration.

Recently, works on active FTC for quadrotor vehicles subjected to actuator partial faults can be found in (Merheb and Noura, 2019; Nian et al., 2020; Ortiz-Torres et al., 2020b; Büyükkabasakal et al., 2017). In (Merheb and Noura, 2019; Nian et al., 2020) the faults were injected only when the vehicle was flying at hover position. To the best of our knowledge, only few experimental validations for a quadrotor flying in a non-hover position have been validated, see (Avram et al., 2017) and (Ortiz-Torres et al., 2020b). In (Ortiz-Torres et al., 2020b), the authors developed a Fault Detection (FD) and accommodation algorithm using nonlinear adaptive estimation techniques. In addition, three observers were considered for the FD: a nonlinear adaptive observer and a linear Proportional-Integral Observer (PIO) applied to a PVTOL - Planar Vertical Take Off and Landing- and a quasi-Linear Parameter Varying (qLPV) for a quadrotor. Due to the complexity of designing, tuning and implementing these controllers, it is difficult to conduct real-time simulations and experiments. Therefore, a simple solution is required. In this paper, we propose a simple and efficient robust control algorithm for handling rotor failures. The control architecture is composed by a nominal controller (e.g. controller of a commercial aerial vehicle) and an observer that simplifies its implementation on real-time scenarios. Regardless of aggressive rotor failures, the nominal controller does not require to be re-tuned. To the best of our knowledge, this is the first time that an uncertainty and disturbance observer is designed using the real control inputs of the system (the actuators). This allows us to design a rotors fault estimator and as well to provide the practical stability of the aerial vehicle when rotors failures are induced. Finally, the proposed scheme is tested in aggressive conditions in numerical simulations and in real-time flights, corroborating and exploiting their robustness properties on rotor's faults. We consider in this work as aggressive conditions, when rotor failures of more than 40% of LoE are induced in a hover and non hover position.

The paper is organized as follows: the preliminaries and problem formulation are given in Section 2. The rotors fault observer is designed in Section 3. Numerical and practical validation of the architecture is carried out and main graphs are illustrated in Section 4. An analysis of the results are given in Section 5. And finally in Section 6, the final conclusions and perspectives of our work are given.

2 Preliminaries & Problem formulation

The model of a quadrotor can be described by representing the vehicle as a $3D$ rigid body, as shown in Fig. 1, and using the Newton-Euler formalism. Therefore, it can be expressed as

$$\begin{aligned} \dot{\boldsymbol{\xi}}(t) &= \mathbf{v}(t), \qquad m\dot{\mathbf{v}}(t) = \mathbf{R}(t)\mathbf{F}(t) + \boldsymbol{d}_{\xi}, \\ \dot{\mathbf{R}}(t) &= \mathbf{R}(t)\hat{\boldsymbol{\Omega}}(t), \quad \mathbf{J}\dot{\hat{\boldsymbol{\Omega}}} = -\boldsymbol{\Omega}(t) \times \mathbf{J}\boldsymbol{\Omega}(t) + \boldsymbol{\tau}(t) + \boldsymbol{d}_{\eta} \end{aligned} \tag{1}$$

where $\boldsymbol{\xi}(t)$ denotes the vector position of the vehicle with respect to the frame $\mathscr{I}$, $\mathbf{v}(t) \in \mathscr{I}$ describes the linear velocity, $\boldsymbol{\Omega}(t)$ represents the angular velocity of the body defined in $\mathscr{B}$, and m is the total mass of the vehicle. The constant moment of inertia is denoted by $\mathbf{J}$ expressed in $\mathscr{B}$, $\boldsymbol{\tau}(t) \triangleq [u_2, u_3, u_4]$ expresses the torques applied in the rigid body, $\hat{\boldsymbol{\Omega}}(t)$ introduces the skew-symmetric matrix of $\boldsymbol{\Omega}(t)$, $\mathbf{R}(t)$ means the rotation matrix from $\mathscr{B}$ to $\mathscr{I}$, and $\mathbf{F}(t) \triangleq [0, 0, u_1]$ are the forces applied to the rigid body. $\mathbf{d}_{\xi}, \boldsymbol{d}_{\eta}$ denotes the exogenous and unknown disturbances.

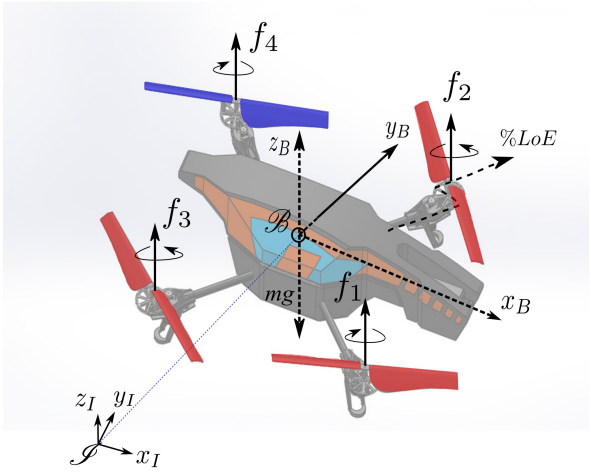

Figure 1: Quadrotor aerial vehicle representation. $\mathscr{I} = \{x_I, y_I, z_I\}$ denotes the inertial frame, and $\mathscr{B} = \{x_B, y_B, z_B\}$ is the body frame attached to the center of mass of the vehicle.

Note that, system (1) is often expressed as

$$\begin{aligned} \dot{\boldsymbol{x}}(t) &= (\mathbf{A} + \Delta\mathbf{A})\,\boldsymbol{x}(t) + (\mathbf{B} + \Delta\mathbf{B})\,\bar{\mathbf{u}}(t) \\ &\quad + \mathbf{f}(\boldsymbol{x}, \bar{\mathbf{u}}, t) + \mathbf{d}(t) \\ \mathbf{y}(t) &= \boldsymbol{x}(t) \end{aligned} \tag{2}$$

where $\boldsymbol{x}(t) \in \mathbb{R}^n$ and $\bar{\mathbf{u}}(t) \in \mathbb{R}^m$ are the state and control variables, $\mathbf{f}(\boldsymbol{x}, \bar{\mathbf{u}}, t) : \mathbb{R}^n \times \mathbb{R} \times \mathbb{R}^+ \to \mathbb{R}^n$ defines a non-linear function, and $\mathbf{d}(t) : \mathbb{R}^+ \to \mathbb{R}^n$. The full state is assumed to be measurable. The state and control matrices are split so that $\mathbf{A}$ and $\mathbf{B}$ are known and $\Delta\mathbf{A}$ and $\Delta\mathbf{B}$ are parametric uncertainties. Moreover, it is assumed that the nonlinear function $\frac{\partial[\mathbf{f}(x,\bar{u})+\mathbf{B}\bar{u}]}{\partial\bar{u}} \neq 0$, for all $(\boldsymbol{x}, \bar{\mathbf{u}}) \in \mathbb{R}^n \times \mathbb{R}^m$.

The equations of the model (1) can be written in the form of (2) as (Bouabdallah et al., 2004b):

$$\mathbf{A} = \begin{bmatrix} 0_6 & I_6 \\ 0_6 & 0_6 \end{bmatrix},\ \mathbf{B} = \begin{bmatrix} 0_6 \\ \bar{\mathbf{B}} \end{bmatrix}, \mathbf{f} = \begin{bmatrix} 0_6 \\ \bar{\mathbf{f}} \end{bmatrix},\ \mathbf{d} = \begin{bmatrix} 0_6 \\ \bar{\mathbf{d}} \end{bmatrix}$$

where $\bar{\mathbf{d}} = [\mathbf{d}_\xi, \mathbf{d}_\eta]^T$, $\bar{\mathbf{B}} = [m^{-1}, m^{-1}, (m^{-1} - g), I_x^{-1}, I_y^{-1}, I_z^{-1}]^T$ and $\bar{\mathbf{f}}$ is composed by $\bar{f}_1 = \frac{\cos\phi\sin\theta\cos\psi + \sin\phi\sin\psi}{m} u_1$, $\bar{f}_2 = \frac{\cos\phi\sin\theta\sin\psi - \sin\phi\cos\psi}{m} u_1$, $\bar{f}_3 = \frac{u_1}{m}(1 - \cos\phi\cos\theta)$, $\bar{f}_4 = \frac{(I_y - I_z)}{I_x}\dot{\theta}\dot{\psi} - \frac{J}{I_x}\dot{\theta}\Omega$, $\bar{f}_5 = \frac{(I_z - I_x)}{I_y}\dot{\psi}\dot{\phi} + \frac{J}{I_y}\dot{\phi}\Omega$ and $\bar{f}_6 = \frac{(I_x - I_y)}{I_z}\dot{\theta}\dot{\phi}$.

An aerial vehicle needs a robust control system to compensate the adverse effects of model uncertainties ($\Delta\mathbf{A}$, $\Delta\mathbf{B}$), unmeasured and nonlinear dynamics ($\mathbf{f}$) and external disturbances ($\mathbf{d}$), such as wind and turbulence (Luque-Vega et al., 2012). These non desired effects can be also produced by actuators fault (damage in the propeller or the motor itself) producing a loss in the efficiency of the vehicle. Voltage variations in battery can also be seen as Loss of Efficiency (LoE) in motors, which is reasonable due to the motor thrusts (Schacht-Rodríguez, 2018).

In this work, the challenge will be to propose a robust control architecture via a rotor fault observer for improving/reinforcing the performance of the closed-loop system when using nominal controllers (linear, nonlinear). This novel control-observer architecture, depicted in Figure 2, is robust with respect to model uncertainties and external disturbances (e.g. wind gust). In addition, it is capable to detect and compensate rotors fault, as loss of efficiency. Our goal is to validate experimentally the proposed architecture in flight tests with critical and non critical scenarios. Note that this architecture is quite different from the traditional Fault Tolerant Control (FTC) schemes because our system is capable to react fast enough to compensate rotors fault, without using the isolation and reconfiguration tasks of the FTC schemes, even when the aerial robot is flying in a non-hover position.

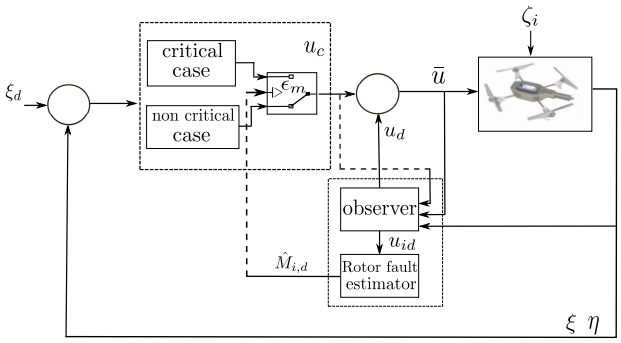

Figure 2: Block diagram of the control structure. u_{id} corresponds to the estimated disturbances, $\hat{M}_{i,d}$ is the rotor faults estimation and ξ_d is the desired position. $\bar{\mathbf{u}}$ represents the vector control input containing the main thrust and the control torques respectively. ζ_i means the external disturbances and ϵ_m symbolizes the desired threshold.

3 Rotors fault observer

Let us consider a reference model as follows

$$\dot{\boldsymbol{x}}_q(t) = \mathbf{A}_q \boldsymbol{x}_q(t) + \mathbf{B}_q \mathbf{r}_q(t) \tag{3}$$

where $\boldsymbol{x}_q \in \mathbb{R}^n$, $\mathbf{A}_q \in \mathbb{R}^{n\times n}$ and $\mathbf{B}_q \in \mathbb{R}^{n\times m}$ are the state reference matrix and the control reference vector, respectively. $\mathbf{r}_q(t)$ is continuous and uniformly bounded command to the system.

Let assume that the desired dynamics of the closed-loop system (1) or (2) are given in terms of the reference model described in (3). Therefore, the goal will be to find a control algorithm such that $\boldsymbol{x} \to \boldsymbol{x}_q$ where $\boldsymbol{x}$ is the real system state and $\boldsymbol{x}_q$ the reference model state. Thus define the error as $\mathbf{e} = \boldsymbol{x}_q - \boldsymbol{x}$. Differentiating the error and using (2) and (3), and adding and subtracting $\mathbf{A}_q\boldsymbol{x}$, it holds

$$\begin{aligned} \dot{\mathbf{e}} &= \mathbf{A}_q\mathbf{e} + \mathbf{A}_q\boldsymbol{x} + \mathbf{B}_q\mathbf{r}_q(t) - (\mathbf{A}+\Delta\mathbf{A})\boldsymbol{x} \\ &\quad -(\mathbf{B}+\Delta\mathbf{B})\bar{\mathbf{u}} - \mathbf{f}(\boldsymbol{x},\bar{\mathbf{u}},t) - \mathbf{d}(t). \end{aligned} \tag{4}$$

Hence, the goal will be that $\mathbf{e} \to 0$ asymptotically. Then, $\bar{\mathbf{u}}$ can be proposed as

$$\mathbf{B}\bar{\mathbf{u}} = (\mathbf{A}_q - \mathbf{A})\boldsymbol{x} + \mathbf{B}_q\mathbf{r}_q(t) - \Delta\mathbf{A}\boldsymbol{x} - \Delta\mathbf{B}\bar{\mathbf{u}} - \mathbf{f} - \mathbf{d} \tag{5}$$

Notice from the above that (5) can be separated in two parts; one concerning the reference tracking performance, that can be defined as $\mathbf{u}_c$, while the second one relating to the unknown dynamics and effects into the system, that will be denoted as $\mathbf{u}_d$. Thus, considering the pseudo-inverse of $\mathbf{B}$ as $\mathbf{B}^+ = (\mathbf{B}^T\mathbf{B})^{-1}\mathbf{B}^T$, (5) becomes

$$\bar{\mathbf{u}} = \mathbf{u}_c + \mathbf{u}_d. \tag{6}$$

with

$$\mathbf{u}_c = \mathbf{B}^+[(\mathbf{A}_q - \mathbf{A})\boldsymbol{x} + \mathbf{B}_q\mathbf{r}_q(t)] \tag{7}$$

and

$$\mathbf{u}_d = \mathbf{B}^+[-\Delta\mathbf{A}\boldsymbol{x} - \Delta\mathbf{B}\bar{\mathbf{u}} - \mathbf{f}(\boldsymbol{x},\bar{\mathbf{u}},t) - \mathbf{d}(t)]. \tag{8}$$

On the one hand, note from (7) that $\mathbf{u}_c(t) = \mathbf{K}\boldsymbol{x}(t) + \mathbf{B}^+\mathbf{B}_q\mathbf{r}_q(t)$, with $\mathbf{K} = \mathbf{B}^+(\mathbf{A}_q - \mathbf{A})$ is the control part for stabilizing the system in ideal conditions, i.e., its linear part. On the other hand, $\mathbf{u}_d$ will contain the observer part and will be the control part for compensating and estimating the inner uncertainties, unknown

dynamics or external perturbations in the system. Let us define the lumped term $\boldsymbol{w} \in \mathbb{R}^m$, containing all the model uncertainties and external disturbances as follows

$$\boldsymbol{w} \triangleq \Delta\mathbf{A}\boldsymbol{x} - \Delta\mathbf{B}\bar{\mathbf{u}} - \mathbf{f}(\boldsymbol{x}, \bar{\mathbf{u}}, t) - \mathbf{d}(t). \tag{9}$$

Assumption 1 *The lumped disturbance $\boldsymbol{w}$ is bounded as well as its derivative*

Observe that (8) is a function of the unknown variables $\Delta\mathbf{A}\boldsymbol{x}, \Delta\mathbf{B}, \bar{\mathbf{u}}, \mathbf{f}(\boldsymbol{x}, \bar{\mathbf{u}}, t), \mathbf{d}(t)$. However, using (2), it can be rewritten as

$$\mathbf{u}_d = \mathbf{B}^+[\mathbf{A}\boldsymbol{x} + \mathbf{B}\bar{\mathbf{u}} - \dot{\boldsymbol{x}}] \tag{10}$$

Intuitively, it indicates that the unknown dynamics and disturbances are related and then can be estimated from the known dynamics of the system and control signal. Following ideas from (Zhong and Rees, 2004), (10) can be approximated by

$$\mathbf{U}_d(s) = \mathbf{G}_f(s)\mathbf{B}^+[\mathbf{A}\mathbf{X}(s) + \mathbf{B}\bar{\mathbf{U}}(s) - s\mathbf{X}(s)] \tag{11}$$

Assume that $G_f(s)$ is a strictly proper low-pass filter with unity steady-state gain and broad enough bandwidth. From assumption 1, the asymptotic stability of the closed-loop system for multi-rotor vehicles can be demonstrated as in (Sanz et al., 2017).

3.1 Rotor fault estimator

To compensate external disturbances affecting the vehicle, the estimation of $\mathbf{u}_d$ with the form in (8) is the only one necessary. This is possible because $\mathbf{u}_d$ is related with the control inputs of the system $\bar{\mathbf{u}}$. Nevertheless, if the goal is to compensate rotor's faults, this control input needs to be reformulated.

The control inputs, u_i, in the quadrotor system are functions of the combination of the motor's forces f_i. From Figure 1, this relation is often given by

$$\bar{\boldsymbol{u}} = \begin{bmatrix} u_1(t) \\ u_2(t) \\ u_3(t) \\ u_4(t) \end{bmatrix} = \begin{bmatrix} 1 & 1 & 1 & 1 \\ l & -l & -l & l \\ l & l & -l & -l \\ -c_{tf} & c_{tf} & -c_{tf} & c_{tf} \end{bmatrix} \begin{bmatrix} f_1(t) \\ f_2(t) \\ f_3(t) \\ f_4(t) \end{bmatrix} \tag{12}$$

where f_i, with $i : 1, \cdots, 4$, are the upward lifting forces generated by motor i, l represents the horizontal distance from the center of mass to the center of a rotor and c_{tf} is the propeller torque coefficient. We assume, in this work, that the thrust of each propeller is directly controlled and attached in the z axis of the vehicle, i.e., the blade flapping effect is not considered.

Notice that (6) and (12) have the same structure, therefore, $\mathbf{u}_c$ and $\mathbf{u}_d$ are also vectors of four components and functions of the forces f_i. In addition, the force i, produced by motor i, can be computed using its angular rate w_{M_i}, such that, $f_i \approx k_f w_{M_i}^2$ with k_f defining an aerodynamic thrust factor.

In real-time validation, the control inputs of the system $\bar{\mathbf{u}}$ are transformed into the real control inputs for each actuator (motors). This is often known as control allocation, where each control input of the system u_i is fused or combined for obtaining the real input for the actuator. For a quadrotor vehicle it is obtained as follows:

$$\mathbf{M} = \mathbf{H}\bar{\mathbf{u}},$$

with

$$\mathbf{M} = \begin{bmatrix} M_1(t) \\ M_2(t) \\ M_3(t) \\ M_4(t) \end{bmatrix}; \qquad \bar{\mathbf{u}} = \begin{bmatrix} u_1(t) \\ u_2(t) \\ u_3(t) \\ u_4(t) \end{bmatrix} = \begin{bmatrix} u_{1c} + u_{1d} \\ u_{2c} + u_{2d} \\ u_{3c} + u_{3d} \\ u_{4c} + u_{4d} \end{bmatrix};$$

and $\mathbf{H}$ denotes the allocation control matrix. This matrix is related with the rotors configuration in the system, for a quadrotor configuration it has the following form

$$\mathbf{H} = \begin{bmatrix} 1 & 1 & 1 & -1 \\ 1 & -1 & 1 & 1 \\ 1 & -1 & -1 & -1 \\ 1 & 1 & -1 & 1 \end{bmatrix}.$$

Hence, $\mathbf{M}$ can be also separated as $\mathbf{M} = \mathbf{M}_c + \mathbf{M}_d$ where the first one corresponding for the values computed with the control law $\mathbf{u}_c$ and the second one is for the disturbances rejection. Then, $\mathbf{M}_d$ is the vector parameter that should compensate the undesired performances in the vehicle.

Analyzing only the disturbance part contribution, it follows that $\mathbf{M}_d = \mathbf{H}\mathbf{u}_d$. Rewriting it, in the scalar form, it follows that

$$\begin{aligned} M_{1d} &= u_{1d} + u_{2d} + u_{3d} - u_{4d}, \\ M_{2d} &= u_{1d} - u_{2d} + u_{3d} + u_{4d}, \\ M_{3d} &= u_{1d} - u_{2d} - u_{3d} - u_{4d}, \\ M_{4d} &= u_{1d} + u_{2d} - u_{3d} + u_{4d}. \end{aligned} \tag{13}$$

From (13), we observe that u_{1d} is common for the four rotors so it can be considered as the altitude disturbance in the vehicle that affects the efficiency of all rotors power at the same time. Therefore, its contribution for detecting if one motor is losing efficiency is less important. Nevertheless, we notice also from (13) that the combination of the terms u_{jd} for $j : 2, 3, 4$; has a severe impact in each rotor. Hence, from the previous analysis, it is possible to propose the following rotors fault estimator:

$$\begin{aligned} \hat{M}_{1d} &= u_{2d} + u_{3d} - u_{4d}, \\ \hat{M}_{2d} &= -u_{2d} + u_{3d} + u_{4d}, \\ \hat{M}_{3d} &= -u_{2d} - u_{3d} - u_{4d}, \\ \hat{M}_{4d} &= u_{2d} - u_{3d} + u_{4d} \\ \hat{M}_{th} &= u_{1d}. \end{aligned} \tag{14}$$

with $\hat{M}_{id}$ is the disturbance parameter estimation for motor i.

In summary, the analysis of equation (14) can be done in two stages:

1. *external/small disturbances* (conventional flights), here the values of $\hat{M}_{id}$ are relatively small but they should not be necessarily null and therefore, the lumped term can be estimated and compensated using (11).
2. *LoE in motors*, in this stage the values of $\hat{M}_{id}$ degrade severally the performance of the vehicle and it can be seen as Loss of Efficiency (LoE) in motors.

From the vehicle configuration and physical characteristics, we observe that if one parameter of $\hat{M}_{id}$ reaches a critical value ϵ_m, the control law will not be capable to keep the vehicle stable at hover position, then an inevitable crash will arise. This critical value is chosen such that a minimal main thrust (u_1) is required to overcome the weight of the vehicle (mg), i.e.,

$$\epsilon_m = \min u_1 = mg + \delta. \tag{15}$$

with δ is a small positive constant. Therefore, two flight modes are proposed:

$$\begin{cases} S_M : \hat{M}_{id} \leq \epsilon_m, \\ E_M : \hat{M}_{id} > \epsilon_m, \end{cases} \tag{16}$$

where S_M and E_M stand for the safe and emergency modes, respectively. Observe also that, all the proposed methodology for estimating the rotors fault in (14) are based on computing $\mathbf{u}_d$ in (10).

On the one hand, remember that from (16), when $\hat{M}_{id} \leq \epsilon_m$, the system stability of (2) with controller (6) can be determined as in (Sanz et al., 2017). On the other hand, $\hat{M}_{id} \geq \epsilon_m$, this stability may not be ensured because the controllability of the system is compromised. Nevertheless, as presented in (Ortiz-Torres et al., 2020), for bigger values of LoE in rotors, it is still possible to guarantee the controllability of the aerial system even if it lost a degree of freedom. More however, a reconfiguration process is necessary.

Thus, for the emergency mode E_M, the control reconfiguration process is given as follows:

1. The controllability of the yaw angle (ψ) is lost when the rotor failure estimation exceeds the threshold.

2. As physical consequence, the vehicle turns along its $z-$axis and then, a desired yaw rate (for producing high velocities) is proposed for controlling the yaw heading angular velocity ($\dot{\psi}$). No re-tuning of the controller is needed in this part.

3. The practical stability of the whole system is recovered trying to reach the desired altitude, z_d. If z_d is not reached quickly the safe landing is activated.

4. The drone lands in a safe mode.

The proof of controllability when an aerial system looses a 1 DoF can be found in (Du et al., 2015; Ortiz-Torres et al., 2020). Thus, $\ddot{\psi} = -k_{\dot{\psi}} e_{\dot{\psi}}$ implies that $\dot{\psi} \to \dot{\psi}_d$ (Castillo et al., 2005). The threshold value ϵ_m is obtained as follows: equation (15) is based on the minimal thrust vector required to overcome the weight of the vehicle (mg). Hence, this value depends of the physical characteristics of the prototype used in experiments. We observed that having bigger values of ϵ_m (or by consequence δ) means the rotor fault estimator, $\hat{M}_{id}$, could be activated with small disturbances/failures in the system (parametric uncertainties, small percentage of LoE in rotors) and thus, the non critical case as well. For the case of the AR.Drone 2.0 quadrotor (the prototype used in experiments) the evolution of ϵ_m with respect to δ is presented in Table 1.

These values can be verified using the Available control authority (ACAI) as explained in (Du et al., 2016) and (Ortiz-Torres et al., 2020a). The conditions showing the controllability analysis of the aerial vehicle when a LoE is induced are also presented in Table 1. From this table, observe that critical LoE corresponds to the case of small values of ϵ_m and the opposite for the non critical case. This is mainly due to the fact that the vector thrust is strongly related to the stability of the aerial vehicle, as described in equation (12). For safety reasons, in this paper, $\epsilon_m = 0.4$ meaning that LoE ≥ 0.4 are considered as a critical rotor fault.

Fault	ϵ_m	δ	LoE	Quadrotor	Quadrotor WY
Non critical	0.72	0.4	0.1	CN	-
	0.62	0.3	0.2	CN	-
	0.52	0.2	0.3	CN	-
	0.42	0.1	0.4	CN	-
Critical	0.32	-0.1	0.5	UCN	CN
	0.22	-0.2	0.6	UCN	CN
	-	-	0.7	UCN	CN
	-	-	0.8	UCN	CN
	-	-	0.9	UCN	CN

Table 1: Quadrotor controllability analysis. CN: controllable, UCN: Uncontrollable and WY: Without yaw.

3.2 Digital implementation

For an easy digital implementation, we use each state separately and represented as two integrators in cascade with the form

$$\dot{\boldsymbol{x}}_j(t) = \mathbf{A}_j \boldsymbol{x}_j(t) + \mathbf{B}_j u_i(t) = \begin{bmatrix} 0 & 1 \\ 0 & 0 \end{bmatrix} \boldsymbol{x}_j(t) + \begin{bmatrix} 0 \\ b_j \end{bmatrix} u_i(t), \tag{17}$$

where $\boldsymbol{x}_j = [x_{j1},\ x_{j2}]^T$ denotes the position and angular velocity of each subsystem $j : x, y, z, \theta, \phi, \psi$ and $i : 1 : 4$. This can be also expressed in discrete time as

$$\begin{aligned} \boldsymbol{x}_j(k+1) &= \mathbf{A}_{zj} \boldsymbol{x}_j(k) + \mathbf{B}_{zj} u_i(k) \\ &= \begin{bmatrix} 1 & T \\ 0 & 1 \end{bmatrix} \boldsymbol{x}_j(k) + \begin{bmatrix} 0 \\ T b_j \end{bmatrix} u_i(k), \end{aligned}$$

being T the sample time used to discretize the system.

Similarly, (10) can be represented in discrete domain time as

$$\mathbf{u}_d(k) = \mathbf{B}^+ [\mathbf{A}_z \boldsymbol{x}(k) + \mathbf{B}_z \bar{\mathbf{u}}(k) - \boldsymbol{x}(k+1)]. \tag{18}$$

Expression (18) is not causal, but it can be approximated by introducing a first-order filter. Then, using the Z transform and taking into account that $\boldsymbol{x}(k+1) = \zeta \boldsymbol{x}(\zeta)$, it yields

$$\mathbf{u}_d(\zeta) = \left(\frac{1 - \frac{T}{T_f}}{\zeta - \frac{T}{T_f}} \right) I \mathbf{B}^+ [\mathbf{A}_z \boldsymbol{x}(\zeta) + \mathbf{B}_z \bar{\mathbf{u}}(\zeta) - \zeta \boldsymbol{x}(\zeta)].$$

where T_f represents the first-order filter parameter and I the identity matrix. From the above expression and rewriting it for each state variable, $\boldsymbol{x}_j$, it follows

$$\mathbf{u}_{id}(\zeta) = \left(\frac{\zeta - 1}{T b_j (\zeta - \frac{T}{T_{fj}})} \right) x_{j2}(\zeta) - \left(\frac{1 - \frac{T}{T_{fj}}}{\zeta - T_{fj}} \right) \bar{\mathbf{u}}_i(\zeta) \tag{19}$$

The above expression can be also represented in discrete time, helping the user its implementation in microcontrollers. Then, it yields

$$\begin{aligned} \mathbf{u}_{id}(k) &= \left(1 - \frac{T}{T_{fj}}\right) \mathbf{u}_{id}(k-1) + \\ &\quad \frac{T}{T_{fj}} \left(\frac{\boldsymbol{x}_{j2}(k) - \boldsymbol{x}_{j2}(k-1)}{b_j T} - \bar{\mathbf{u}}_i(k-1) \right), \end{aligned}$$

where i stands for each state variable of component of the vector: $\bar{\boldsymbol{u}} = \left[u_1(t),\ u_2(t),\ u_3(t),\ u_4(t)\right]^T$.

4 Numerical and practical validation

The proposed robust control scheme in (6) - (14) was validated in numerical simulations and real-time experiments. We focus on validating it when the aerial vehicle suffers undesired dynamics produced by rotor failures. Our model for each axis is a double integrator (17), where b_i is obtained experimentally. The control parameters for simulations and experiments are presented in the Table 2. Here, k_{p_i} and k_{d_i}, express the control parameters $\mathbf{K} = \left[k_{p_i},\ k_{d_i}\right]^T$ for obtaining the desired reference model:

$$A_{q_i} = \begin{bmatrix} 0 & 1 \\ -a_{q1_i} & -a_{q2_i} \end{bmatrix}, B_{q_i} = \begin{bmatrix} 0 \\ b_{q_i} \end{bmatrix}$$

Two scenarios are proposed for simulations and experimental tests. They are defined as follows:

Table 2: Control parameters for simulations and experimental tests. The parameters k_{p_i} and k_{d_i} are positive diagonal matrices for stabilizing the system in nominal conditions. The parameters b_i, a_{q1_i}, a_{q2_i} and b_{q_i} where obtained experimentally using the Pseudo Random Binary Sequence (PRBS) method. The parameter T_{fi} is chosen as $0 < T_{fi} < 1$.

Parameter	ϕ, θ	ψ	x, y	z
k_{p_i}	0.8	0.6	0.17	0.3
k_{d_i}	0.1	0.2	0.13	0.1
b_i	140	44	10	5
T_{fi}	0.1	0.5	0.5	0.3
a_{q1_i}	112	26.4	1.7	1.5
a_{q2_i}	14	8.8	1.3	0.5
b_{q_i}	112	26.4	1.7	1.5

Scenario A - The first one is when the vehicle is moving from a point A to point B and a rotor fault occurs ($LoE < \epsilon_m$). It is named *"Rotor fault in non hover position"*. This scenario is for flights in safe mode (S_M) or non critical case. Here, the architecture can attenuate internal/external disturbances such as: wind, uncertainties into the model, etc, in such way that the practical stability of the quadrotor can be guaranteed.

Scenario B - The second is when the aerial vehicle is at hover and a critical rotor fault occurs ($LoE \geq \epsilon_m$). This last one is named *"Critical rotor fault"*. Here, the emergency mode (E_M) or critical case, is used to detect important system degradation performance and assure a safe landing. In this critical case, often used in rotors failures, one degree of freedom is lost into the system and the control architecture is reconfigured for maintaining the aerial drone in flight or ensuring a safe landing.

4.1 Simulations

As previously explained, two scenarios are introduced for numerical validation. The first one consists in reducing the effectiveness in motor M_1 when the aerial robot is performing a non hover position (Scenario A). For the second one (Scenario B), a critical LoE in M_1 is injected when the vehicle is at hover position such that the system losses a degree of freedom. In this case, the emergency landing is required. Both scenarios are compared with the nominal controller $\mathbf{u}_c$, the proposed robust architecture $\bar{\mathbf{u}}$ and an active fault tolerant control $\mathbf{u}_{FTC}$ as proposed in (Ortiz-Torres et al., 2020).

4.1.1 Scenario A : Rotor fault in a non hover position

In this scenario, the effectiveness of M_1 is reduced 30% while the vehicle is flying from points A to B with coordinates $\xi(t_0 = 0) = [-2,\ 0,\ 2]^T$m and $\xi_d = [3,\ 0,\ 2]^T$m, respectively. In Figures $3 - 5$, the performance of the vehicle in 3D space when performing the desired task is addressed. Remark that when using the proposed architecture and injecting the fault, the whole system overcomes it and converges to the desired final point (solid line). In other case, when using only the nominal controller $\mathbf{u}_c$ or the active FTC $\mathbf{u}_{FTC}$, the performance of the vehicle is degraded (dashed and dash-dotted lines, respectively).

4.1.2 Scenario B : A critical rotor fault (E_M)

In this scenario, the aerial vehicle is at hover at the position $\xi = [0,\ 0,\ 2]^T$m. M_1 is then degraded 60% of its effectiveness at $t = 4.5s$. Here, the fault estimation exceeds the threshold, and then, the control algorithm switches into emergency mode. In the reconfiguration control, the yaw angle is lost and the desired yaw velocity is chosen as $\dot{\psi}_d = 10$ rad/s, then a desired reference of $\xi_d = [1.5,\ 0,\ 2]^T$m at $t = 21s$ is set for the safety landing. Figures $6 - 8$ shows the performance of the quadrotor subject to a critical rotor failure. From thess figures, we notice that when the fault is injected instantaneously the vehicle crashes when using only the nominal controller $\mathbf{u}_c$. However, when using the proposed control scheme $\bar{\mathbf{u}}$ and the active FTC $\mathbf{u}_{FTC}$, the quadrotor recovers quickly its altitude (at $t = 6s$). For the active FTC case, the performance is harshly degraded in all axes.

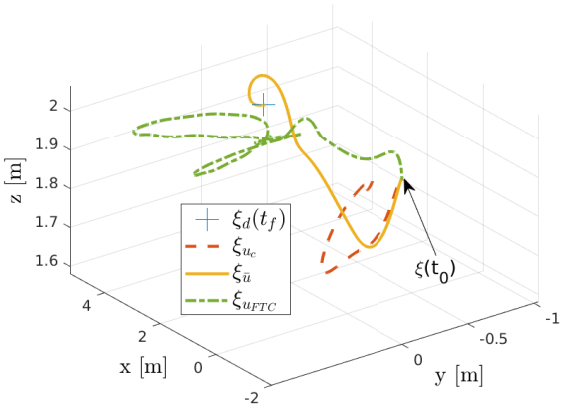

Figure 3: Scenario A - simulation: Quadrotor position performance when using a nominal controller, the proposed architecture and an active FTC. Notice when using the nominal controller $\mathbf{u}_c$, the performance is degraded and thus the error increases.

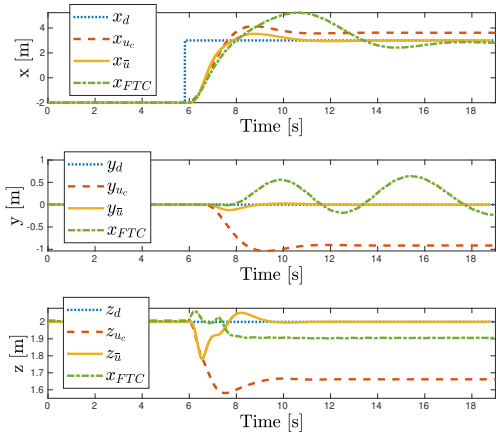

Figure 4: Scenario A - simulation: Position performance of the vehicle using the control algorithms, $\mathbf{u}_c$, $\bar{\mathbf{u}}$, and $\mathbf{u}_{FTC}$. Observe the controller $\mathbf{u}_{FTC}$ converge to the desired position (x and $z-$ axes) but the performance is degraded with some oscillations in the $y-$ axis.

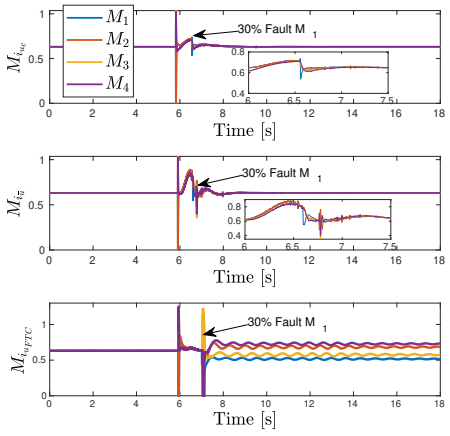

Figure 5: Scenario A - simulation: Rotors control action's performances, when a LoE of 30% in M_1 is applied during a non hover position. Notice the oscillations in the case of $M_{i_{\mathbf{u}_{FTC}}}$. This are mainly due to the degraded system's performance, as can be verified in Figure 4.

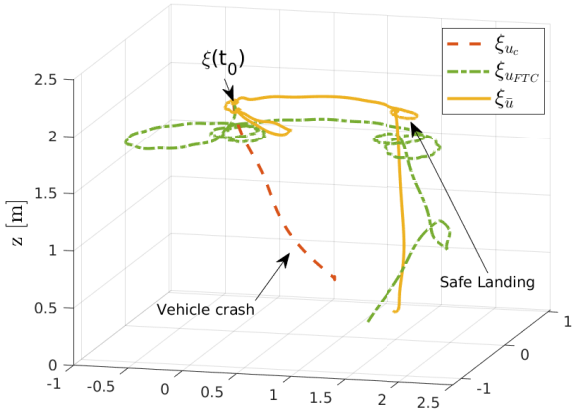

Figure 6: Scenario B - simulation : Quadrotor position performance of the vehicle using the control algorithms, $\mathbf{u}_c$ and $\bar{\mathbf{u}}$, and flying at hover when a critical failure of 60% of LoE is applied in M_1.

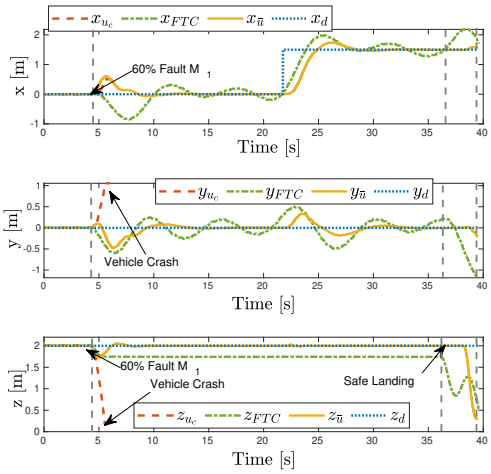

Figure 7: Scenario B - simulation : Performance of the vehicle positions using the control algorithms, $\mathbf{u}_c$ and $\bar{\mathbf{u}}$, and flying at hover when a critical failure is applied in M_1. Notice when using $\mathbf{u}_{FTC}$ the systems recovers the practical stability but with a degraded performance.

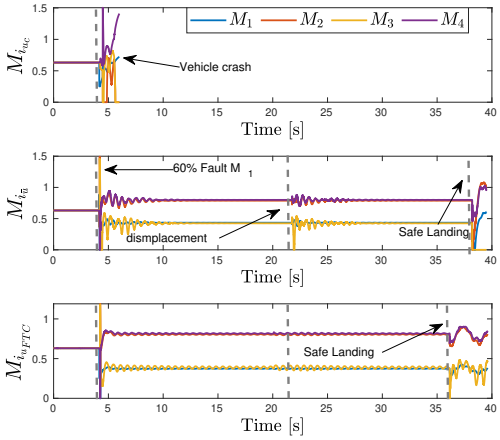

Figure 8: Scenario B - simulation: Rotors control action's performances, when a LoE of 60% in M_1 is applied. Remark the reconfiguration process between $\mathbf{u}_{FTC}$ and $\bar{\mathbf{u}}$. One changes immediately the control gains and lose 1 dof while the other is only losing the yaw control.

4.2 Experimental results

Scenarios A and B were replicated in real-time tests. The experimental tests were performed in a quadrotor vehicle type AR Drone 2. Its firmware was modified to work under the software FL-air which is open source and runs on a Linux-based operating system, capable of implementing a wide range of control schemes, see (Lab, 2012). An OptiTrack motion capture system was used to estimate the vehicle's position, while its internal Inertial Measurement Unit (IMU) measures its orientation and angular rates.

4.2.1 Scenario A : Rotor fault in a non hover position

Similarly that in simulation, the aerial vehicle moves in straight line from points A to B with coordinates $\xi(t_0) = [-2,\ 0,\ 2]^T$m and $\xi_d = [3,\ 0,\ 2]^T$m, respectively. On time $t = 6s$, the LoE in M_1 is reduced 30%. Figure 9 shows the behaviors of the vehicle in 3D space when performing the desired task and using two controllers. Observe that when the fault is injected and the proposed architecture is applied, the quadrotor overcomes it and converges to the desired final point. Otherwise, the performance of the vehicle is degraded. In Figure 10, the estimation of the motors fault is presented. Notice that the observer keeps estimating the fault even if it was compensated. Similarly, in Figure 11, the motor control input performances are depicted.

A video of the experimental results can be seen in
https://youtu.be/UYk1AnhXPgs.

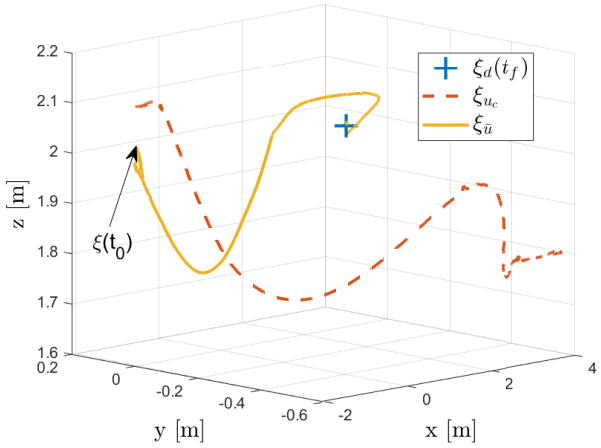

Figure 9: Scenario A - flight tests: Position performance of the vehicle when using the nominal controller and the proposed architecture, and a rotor fault is induced in a non hover position. https://youtu.be/UYk1AnhXPgs

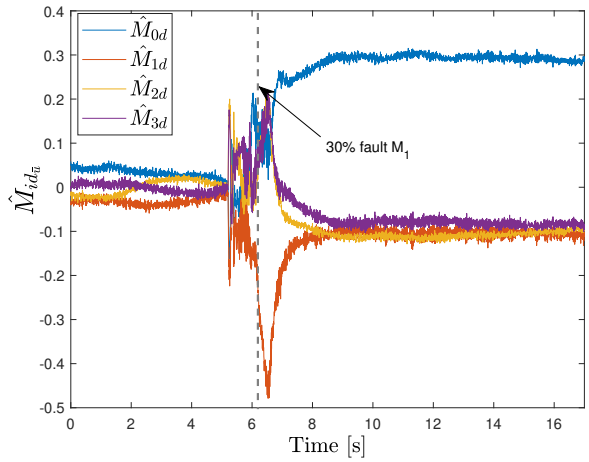

Figure 10: Scenario A - flight tests: Rotors fault estimations $\hat{M}_{id}$, $i = 1, 2, 3, 4$.

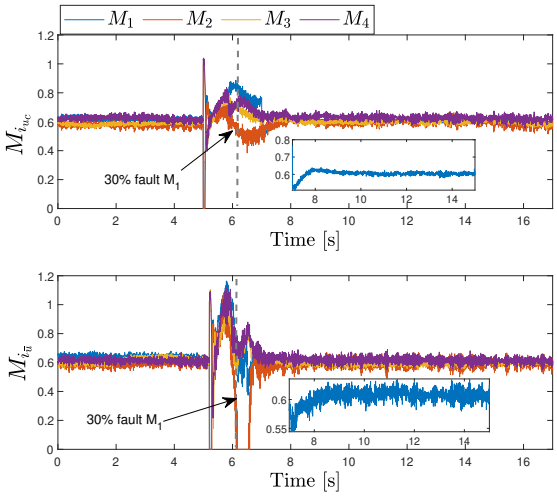

Figure 11: Scenario A - flight tests: Rotors control action's performances, when a LoE of 30% in M_1 is applied during a non hover position.

4.2.2 Scenario B : A critical rotor failure

When a quadrotor is performing a task and a critical rotor fault occurs, the quadrotor will not always land safely. The goal of these tests are to present the performance of the vehicle when a critical fault appears and while it is flying in zones where a safety landing immediately is not possible. Thus, searching for a safe zone must be performed. Nevertheless, we observed that with a LoE of 60% in a motor, the aerial vehicle was not capable to reach the desired altitude for moving in the plane $x-y$ and automatically the safe landing was activated. For demonstrating that it is possible to move the quadrotor in the plane $x-y$ with a critical fault and losing a degree of freedom, we have included for this scenario two cases. They are defined as follows

1. Scenario B - case A : A critical fault (50% LoE) is induced in a motor when the vehicle is at hover position.
2. Scenario B - case B : A critical fault (60% LoE) is applied in a motor and the emergency landing is applied.

Case A : Searching for a safe zone for landing

In this case, the quadrotor is located at $\xi(t_0) = [0, 0, 2]^T$m, and the energy in motor M_1 is degraded of 50%. Then, according to the control reconfiguration procedure, the control law switches to the emergency mode. Here, the position yaw control is lost and only the yaw rate can be controlled. Once the drone attitude is recovered reaching its desired altitude z_d, a safe set-point; $\xi_d = [2, 0, 2]^T$m is sent to the quadrotor simulating a coordinate where the vehicle can be landed in safety mode.

In Figure 12 the 3D performance of the vehicle when a critical fault injected in motor M_1 is depicted. Notice here that, on the one hand, when the fault is injected, the nominal controller is not enough to compensate it and the system performance is harshly degraded, making the drone crashes (dotted line). On the other hand, when the aerial drone is flying with the proposed control scheme, its performance is barely degraded such that safe displacements and a safe landing are possible. Figure 13 presents the behavior of the vehicle in the three axes when the fault in motor M_1 is applied.

Observe that, when the virtual rotor fault is injected, the performance of the vehicle when using the state feedback (nominal) controller is degraded. However, in the same figure in the $z-$ axis at $4 \leq t \leq 6$, we

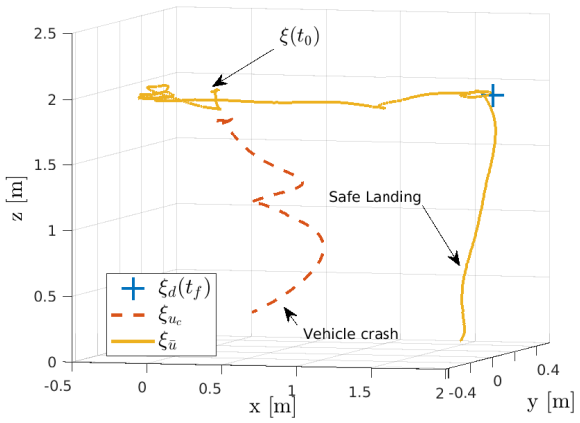

Figure 12: Scenario B - case A - flight tests : Performance of the aerial vehicle when a motor losses effectiveness of 50%. https://youtu.be/MWMvRoSPLfg

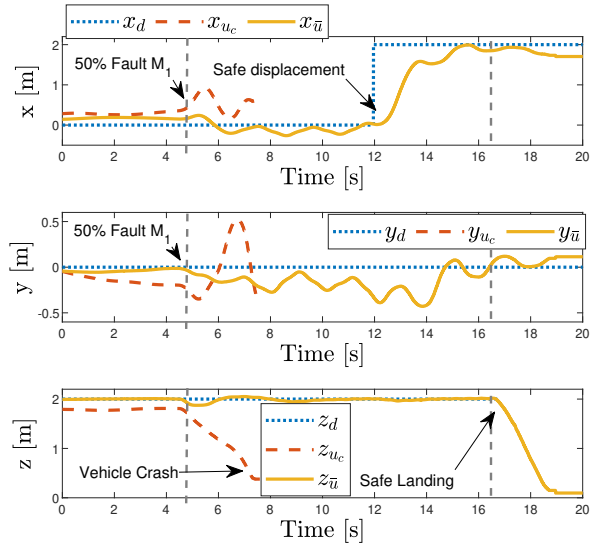

Figure 13: Scenario B - case A - flight tests : Performance of the quadcopter position subject to a critical rotor fault of 50% in M_1.

note that when using the proposed scheme the performance of the drone is barely degraded. x and y axis vary as the quadrotor turns on its own axis and simultaneously, controlling the error position. The safe reference is sent at $t = 12$s and once the vehicle arrives, the safe landing can be achieved. The performance of the proposed rotor fault estimator is shown in Figure 14. From this figure, we can state that the fault was injected at $t = 4.5s$ and that the performance of the rotor fault observer was good regardless of the failure.

In Figure 15, the performances of the motors M_i subject to a rotor fault of 50% of LoE in M_1 are depicted. Notice that once the fault is injected, the effectiveness range in motor M_1 is reduced 50%. In addition, we remark that the motor M_4 turns off for some milliseconds (for compensating M_1) and, motors M_2 and M_3 increases its velocity to make possible the yaw velocity control. A video of the experimental results can be seen in https://youtu.be/MWMvRoSPLfg.

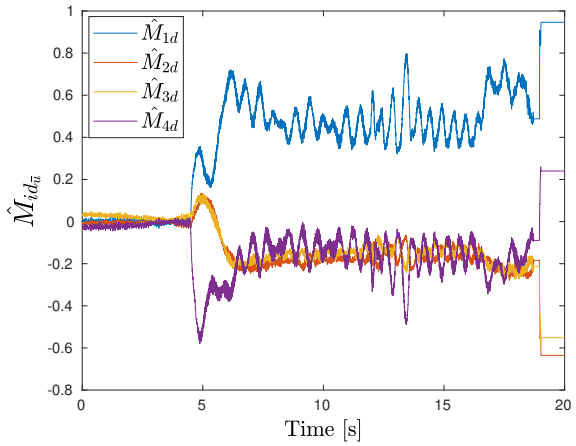

Figure 14: Scenario B - case A - flight tests : Rotors faults estimations $\hat{M}_{id}$, $i : 1, \cdots, 4$.

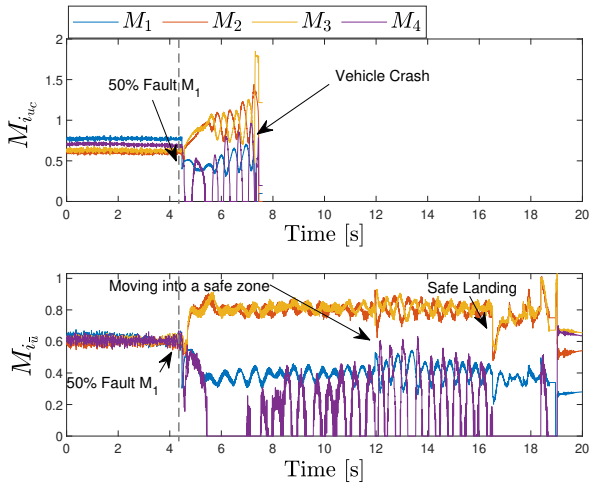

Figure 15: Scenario B - case A - flight tests : Rotors control action's performances when a critical fault of 50% in M_1 is applied.

Case B : Critical rotor fault with emergency landing

In order to keep the safety operation of the vehicle, an emergency landing is a prioritized flight mode made by an aircraft in response to an imminent or ongoing threat, e.g. rotors failures. This experiment shows the performance of the drone when a LoE of 60% is induced in a motor. Thus, the scenario is set as follows: the drone is flying at hover $\xi = [0, 0, 2]^T$m, this position is taken as its initial position $\xi_{t_0=0}$, at time $t = 3.9$s, the virtual failure in M_1 is applied and the vehicle performance degraded. A video of the experimental results can be seen in https://youtu.be/WS5-zpx8S4o.

Notice from Figure 16 that when using only the nominal controller, the robot performance is instantly degraded and it crashes (dotted line). Nevertheless, when using the proposed architecture, the rotor fault observer estimates the motor fault that is compared with the threshold. As the threshold is overpassed, the control scheme switches into the emergency mode. In this mode, the controllability of the yaw angle is lost, and only the yaw velocity control is available. This allows to recover the quadrotor attitude performance and the desired altitude. Nevertheless the aerial robot begins to lose altitude and then the condition for an emergency landing is activated. Thus, at the end, the quadrotor lands safely (solid line). In Figure 17, the estimations of $\hat{M}_{id}$ are depicted. Notice here that their values oscillate after time $t = 4.2$s and they are produced when the aerial robot is turning on its vertical axis.

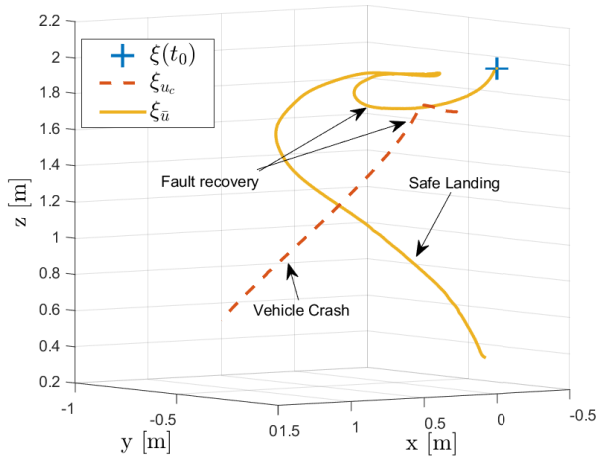

Figure 16: Scenario B - case B - flight tests : Position performance of the vehicle when using the nominal controller and the proposed architecture, and a critical rotor fault is induced. https://youtu.be/WS5-zpx8S4o

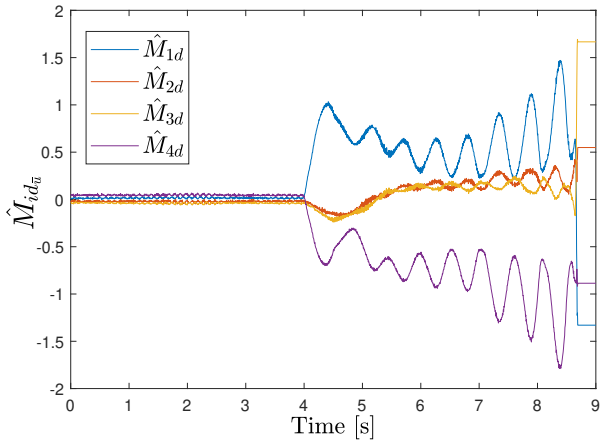

Figure 17: Scenario B - case B - flight tests : Rotors faults estimations $\hat{M}_{id}$, $i : 1, \cdots, 4$.

In Figure 18, the motors performances are illustrated. Remark that M_1 has 40% of its effectiveness when the failure is applied, and then M_4 stops working for short intermittent milliseconds for compensating effectiveness in M_1. We also observe that M_2 and M_3 increase their effectiveness to recover the main thrust and recover the desired altitude, but it produces that the vehicle turns on its vertical axis.

5 Discussion

In this section, we analyse the performance of the proposed architecture against to a nominal controller in three experimental scenarios. For the performance analysis, we compute the Integral Absolute Error (IAE) and the Root Mean Square Error (RMSE) indices. A summary of the analysis of the three experimental tests is presented in Table 3. Note that all the experiments were developed using the same control gains, i.e., re-tuning these variables was not needed. Concerning the steady state regime, from Table results, it can be observed that the proposed robust control scheme achieves the best performance in all the axes. Nevertheless, it is true that is possible to have a better performance for the nominal controller but in this case, re-tuning the control variables most be done for each experiment.

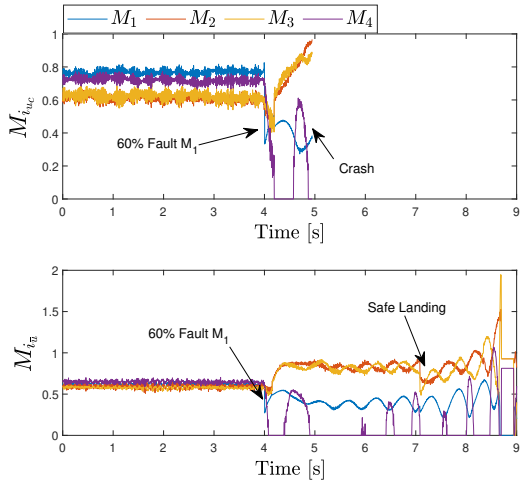

Figure 18: Scenario B - case B - flight tests : Rotors control action's performances, when a critical fault of 60% in M_1 is applied.

Table 3: Performance analysis of the three experiments. "S_A- ft" means Scenario A -flight tests, "S_B - C_A - ft" denotes Scenario B - Case A - flight tests and "S_B - C_B - ft" describes Scenario B - Case A - flight tests.

		S_A - ft		S_B - C_A - ft		S_B - C_B - ft	
		IAE	RMSE	IAE	RMSE	IAE	RMSE
z	u_c	3.34	0.19	inf	inf	inf	inf
	$\bar{u}$	0.39	0.04	1.52	0.41	1.8	0.35
x	u_c	13.02	1.18	inf	inf	inf	inf
	$\bar{u}$	5.29	1.02	5.55	0.46	2.17	0.24
y	u_c	6.01	0.38	inf	inf	inf	inf
	$\bar{u}$	0.35	0.04	1.49	0.22	0.98	0.09

Regarding the control design, tuning and the implementation effort, the nominal controller is easier to tune because its structure can be seen as a simple controller. Our scheme is composed mainly by an observer, a simple reference model of the vehicle and a band-pass filter. All these parameters need to be obtained experimentally in order to have a well approximation of the system. Once the observer is well-tuned for the prototype, it can be used with almost all kind of controllers. The advantage of using the proposed scheme is that it contains an immediate and smooth control action when undesired dynamics appears, especially rotors fault. This can be verified in Table 3, column two and three, where it can be observed that, using only a nominal controller, when a critical rotor fault is injected, it wont be enough to overcome it. Nevertheless, the good performance of the system is guaranteed for the proposed control scheme when critical fault occurs. As all kind of control schemes, there are some limitations that are related with the physical characteristics of the prototype. For example, observe from real-time flight tests that when injecting critical faults more than 70%, the observer sends the respective compensation which exceeds the capacity of effectiveness of all the motors, such that the quadrotor becomes unstable. This is mainly due the fact, the observer does not take into account the limit of operating range of the rotors.

In addition, the Total Variation (TV) of the control input ($TV = \sum_{i=1}^{i=\infty} |u_{i+1} - u_i|$) is used as a measure of the control effort. This index can easily show the aggressively of the controller and can be seen as a measurement of the energy used by the control action. In Table 4, scenario A, the TV of the flight tests is presented. Remark from Figure 19, a similar performance of both controllers. The $\mathbf{u}_c$ controller has a lower TV as a result of that the designed controller is not aggressive as the $\bar{\mathbf{u}}$, but with the lack of the disturbance rejection property, since the $\mathbf{u}_c$ cannot deal with the set-point tracking problem in the presence of faults.

Table 4: Total Variation (TV) of the control inputs.

Scenario A - flight tests								
	u_2	u_3	u_4	u_1	M_1	M_2	M_3	M_4
u_c	26.80	39.43	95.11	4.72	64.68	116.12	54.06	89.43
$\bar{u}$	46.62	65.33	112.80	6.52	76.10	150.75	58.20	117.04
Scenario B - case A - flight tests								
	u_2	u_3	u_4	u_1	M_1	M_2	M_3	M_4
u_c	inf (17.35)	inf (29.13)	inf (32.59)	inf (4.70)	inf (26.36)	inf (29.28)	inf (34.76)	inf (29.47)
$\bar{u}$	30.03 (21.54)	68.45 (32.14)	89.03 (40.61)	10.33 (6.07)	58.05 (31.39)	76.19 (37.62)	69.95 (36.02)	114.97 (40.80)
Scenario B - case A - flight tests								
	u_2	u_3	u_4	u_1	M_1	M_2	M_3	M_4
u_c	inf (10.42)	inf (11.78)	inf (17.54)	inf (1.12)	inf (9.67)	inf (20.91)	inf (16.73)	inf (15.56)
$\bar{u}$	26.31 (12.31)	32.52 (14.90)	38.88 (18.68)	4.45 (1.98)	24.22 (12.75)	53.78 (27.51)	34.06 (20.09)	37.66 (18.64)

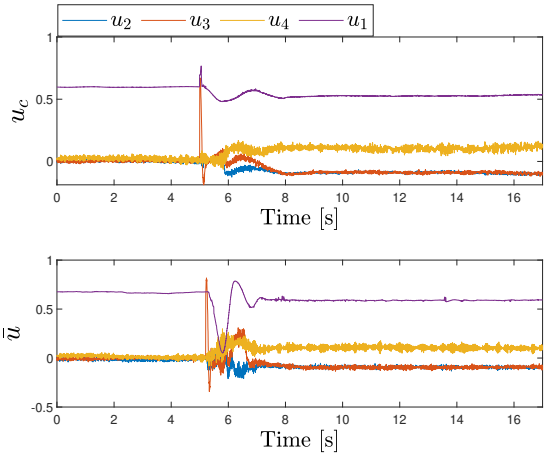

Figure 19: Control inputs $\mathbf{u}_c$ and $\bar{\mathbf{u}}$ of the flight tests for scenario A.

Moreover, based on the performance of the control laws depicted on Figure 20, the TV of the scenario B - case A is presented in Table 4. In contrast to the previous cases, the $\mathbf{u}_c$ controller presents an infinity TV when the fault was injected since the system becomes unstable. This is mainly due that the control algorithm is not robust enough to reject this kind of disturbances. However, the $\bar{\mathbf{u}}$ control can overcome the fault while the drone continue flying safely; the safe landing can be carried-out.

Finally, in Table 4, scenario B, the TV for the experiment of the case B is provided. In this experiment, an aggressive fault was introduced, as can be observed in Figure 21. Therefore, the $\mathbf{u}_c$ controller is not able to continue flying and thus, it becomes unstable such that, the TV becomes infinity. The $\bar{\mathbf{u}}$ controller is able to overcome this problem since is prepared to deal with this kind of high disturbances. We show in parenthesis, the TV of these last two experiments, before the faults were injected.

6 Conclusions

In this work, we proposed a novel robust control architecture based on an observer and a nominal controller. This architecture includes a rotor observer to detect and estimate external disturbances or undesired dynamics, such as rotor failures. Thus, the aerial vehicle is capable to continue flying safely even when rotor faults are encountered.

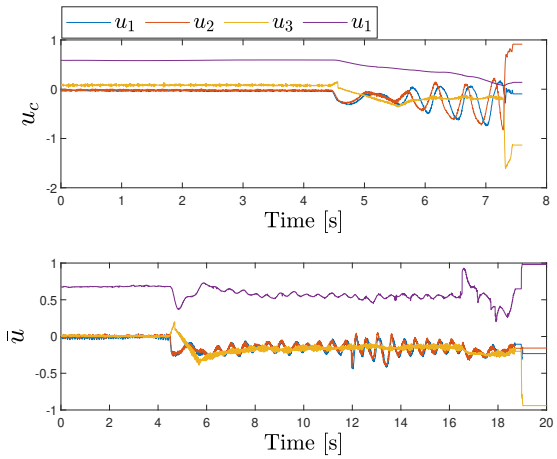

Figure 20: Control inputs $\mathbf{u}_c$ and $\bar{\mathbf{u}}$ of the experiment for scenario B - case A.

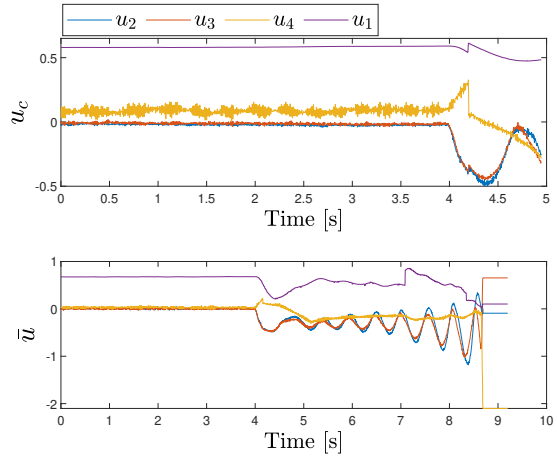

Figure 21: Control inputs $\mathbf{u}_c$ and $\bar{\mathbf{u}}$ of the experiment for scenario B - case B.

Simulations and experimental tests were carried-out for validating the performance of the architecture. We focused these experiments on rotor failures. Three different experiments were proposed to validate the performance of the control architecture in real time; a rotor failure in a non hover position (scenario A), a critical rotor fault with safe displacement and emergency landing (scenario B - case A) and, a critical rotor fault with forced landing (scenario B - case B). In scenario A, a fault of 30% less of the effectiveness of motor M_1 was injected, while the vehicle was moving. For the scenario B - case A, a fault of 50% in motor M_1 was induced. We showed that even when a critical fault occurs, it is possible to move the vehicle to a safe zone and thus land in a safety way. In the scenario B - case B, a critical fault of 60% of the effectiveness of motor M_1 was injected while the vehicle was at hover position. Thus, a safe landing was required.

The analysis of the experimental and simulations results have shown the high performance capacity on rotor faults rejection when using the proposed control scheme and a smoother convergence to the desired reference and low computational cost. Therefore, our approach is a good solution for missions when a rotor failure appears in flight. The experimental comparison of the proposed robust control against active fault tolerant controllers, tracking problems when total rotor faults occurs or even aggressive intermittent wind-gust will be considered as a future work.

A video of the whole experimental results can be seen in https://youtu.be/26PXARrL3V0.

Acknowledgment

This work was supported by CONACyT (Consejo Nacional de Ciencia y Tecnología), Mexico. This work has been also sponsored by the French government research programm Robotex Equipment of Excellence (ANR-10-EQPX-44), the Spanish Ministry of Science, Innovation and Universities, Programme "Estancias de profesores e investigadores senior en centros extranjeros, incluido el Programa Salvador de Madariaga 2019, PRX19/00411". The supports are gratefully acknowledged.

References

Abaunza, H. and Castillo, P. (2019). Quadrotor aggressive deployment, using a quaternion-based spherical chattering-free sliding-mode controller. *IEEE Transactions on Aerospace and Electronic Systems*, 56(3):1979–1991.

Amin, R., Aijun, L., and Shamshirband, S. (2016). A review of quadrotor UAV: control methodologies and performance evaluation. *International Journal of Automation and Control*, 10(2):87–103.

Arıcı, M. and Kara, T. (2020). Robust adaptive fault tolerant control for a process with actuator faults. *Journal of Process Control*, 92:169–184.

Avram, R. C., Zhang, X., and Muse, J. (2017). Quadrotor actuator fault diagnosis and accommodation using nonlinear adaptive estimators. *IEEE Transactions on Control Systems Technology*, 25(6):2219–2226.

Balaguer, V., Gonzalez, A., Garcia, P., and Blanes, F. (2021). Enhanced 2-DOF PID controller tuning based on an uncertainty and disturbance estimator with experimental validation. *IEEE Access*.

Betancourt-Vera, J., Balaguer, V., Castillo Garcia, P., Garcia Gil, P., and Lozano, R. (2020). Robust linear control scheme for nonlinear aerial systems: an experimental study on disturbance rejection. In *23rd International Conference on Intelligent Transportation Systems (ITSC'20)*, Rhodes, Greece.

Betancourt-Vera, J., Castillo, P., Lozano, R., and Vidolov, B. (2018). Robust control scheme for trajectory generation and tracking for quadcopters vehicles: Experimental results. In *2018 International Conference on Unmanned Aircraft Systems (ICUAS)*, pages 1118–1124. IEEE.

Bouabdallah, S., Noth, A., and Siegwart, R. (2004a). PID vs LQ control techniques applied to an indoor micro quadrotor. In *2004 IEEE/RSJ International Conference on Intelligent Robots and Systems (IROS)(IEEE Cat. No. 04CH37566)*, volume 3, pages 2451–2456. IEEE.

Bouabdallah, S., Noth, A., Siegwart, R., and Siegwan, R. (2004b). PID vs LQ control techniques applied to an indoor micro quadrotor. *2004 IEEE/RSJ International Conference on Intelligent Robots and Systems (IROS) (IEEE Cat. No.04CH37566)*, 3:2451–2456.

Büyükkabasakal, K., Fi̇dan, B., and Savran, A. (2017). Mixing adaptive fault tolerant control of quadrotor uav. *Asian Journal of Control*, 19(4):1441–1454.

Castillo, A., Sanz, R., Garcia, P., and Albertos, P. (2016). A quaternion-based and active disturbance rejection attitude control for quadrotor. In *2016 IEEE International Conference on Information and Automation (ICIA)*, pages 240–245. IEEE.

Castillo, A., Sanz, R., Garcia, P., Qiu, W., Wang, H., and Xu, C. (2019). Disturbance observer-based quadrotor attitude tracking control for aggressive maneuvers. *Control Engineering Practice*, 82:14–23.

Castillo, P., Lozano, R., and Dzul, A. (2005). Stabilization of a mini rotorcraft with four rotors: Experimental implementation of linear and nonlinear control laws. *IEEE Control Systems Magazine*, 25(6):45–55.

Cavanini, L., Ippoliti, G., and Camacho, E. F. (2021). Model predictive control for a linear parameter varying model of an UAV. *Journal of Intelligent & Robotic Systems*, 101(3):1–18.

Chen, W.-H., Yang, J., Guo, L., and Li, S. (2015). Disturbance-observer-based control and related methods—an overview. *IEEE Transactions on Industrial Electronics*, 63(2):1083–1095.

Comert, Ceren and Kasnakoglu, C. (2017). Comparing and developing PID and sliding mode controllers for quadrotor. *International Journal of Mechanical Engineering and Robotics Research*, 6(3):194–199.

Dhadekar, D. D., Sanghani, P. D., Mangrulkar, K., and Talole, S. (2021). Robust control of quadrotor using uncertainty and disturbance estimation. *Journal of Intelligent & Robotic Systems*, 101(3):1–21.

Du, G.-X., Quan, Q., and Cai, K.-Y. (2015). Controllability analysis and degraded control for a class of hexacopters subject to rotor failures. 78(1).

Du, J., Hu, X., Krstić, M., and Sun, Y. (2016). Robust dynamic positioning of ships with disturbances under input saturation. *Automatica*, 73:207–214.

Gracia, L., Solanes, J. E., Muñoz-Benavent, P., Miro, J. V., Perez-Vidal, C., and Tornero, J. (2018). Adaptive sliding mode control for robotic surface treatment using force feedback. *Mechatronics*, 52:102–118.

Gu, W., Valavanis, K. P., Rutherford, M. J., and Rizzo, A. (2020). UAV model-based flight control with artificial neural networks: A survey. *Journal of Intelligent & Robotic Systems*, pages 1–23.

Guo, L. and Cao, S. (2014). Anti-disturbance control theory for systems with multiple disturbances: A survey. *ISA transactions*, 53(4):846–849.

Han, J. (2009). From PID to active disturbance rejection control. *IEEE transactions on Industrial Electronics*, 56(3):900–906.

Jia, Z., Yu, J., Mei, Y., Chen, Y., Shen, Y., and Ai, X. (2017). Integral backstepping sliding mode control for quadrotor helicopter under external uncertain disturbances. *Aerospace Science and Technology*, 68:299–307.

Kerr, C., Jaradat, R., and Hossain, N. U. I. (2020). Battlefield mapping by an unmanned aerial vehicle swarm: Applied systems engineering processes and architectural considerations from system of systems. *IEEE Access*, 8:20892–20903.

Lab, H. (2012). FL-AIR framework. accessed: Feb. 27, 2020. [online].

Li, S., Yang, J., Chen, W.-H., and Chen, X. (2011). Generalized extended state observer based control for systems with mismatched uncertainties. *IEEE Transactions on Industrial Electronics*, 59(12):4792–4802.

Lu, Q., Ren, B., and Parameswaran, S. (2020). Uncertainty and disturbance estimator-based global trajectory tracking control for a quadrotor. *IEEE/ASME Transactions on Mechatronics*.

Luque-Vega, L., Castillo-Toledo, B., and Loukianov, A. G. (2012). Robust block second order sliding mode control for a quadrotor. *Journal of the Franklin Institute*, 349(2):719 – 739. Advances in Guidance and Control of Aerospace Vehicles using Sliding Mode Control and Observation Techniques.

Lyu, P., Lai, J., Liu, J., Liu, H. H., and Zhang, Q. (2017). A thrust model aided fault diagnosis method for the altitude estimation of a quadrotor. *IEEE Transactions on Aerospace and Electronic Systems*, 54(2):1008–1019.

Menouar, H., Guvenc, I., Akkaya, K., Uluagac, A. S., Kadri, A., and Tuncer, A. (2017). UAV-enabled intelligent transportation systems for the smart city: Applications and challenges. *IEEE Communications Magazine*, 55(3):22–28.

Merheb, A.-R. and Noura, H. (2019). Active fault-tolerant control of quadrotor uavs based on passive controller bank. In Rizk, R. and Awad, M., editors, *Mechanism, Machine, Robotics and Mechatronics Sciences*, pages 231–241. Springer International Publishing.

Miranda-Colorado, R. and Aguilar, L. T. (2019). Robust PID control of quadrotors with power reduction analysis. *ISA transactions*.

Nian, X., Chen, W., Chu, X., and Xu, Z. (2020). Robust adaptive fault estimation and fault tolerant control for quadrotor attitude systems. *International Journal of Control*, 93(3):725–737.

Ortiz, J. P., Minchala, L. I., and Reinoso, M. J. (2016). Nonlinear robust H-infinity PID controller for the multivariable system quadrotor. *IEEE Latin America Transactions*, 14(3):1176–1183.

Ortiz-Torres, G., Castillo, P., Sorcia-Vázquez, F. D., Rumbo-Morales, J. Y., Brizuela-Mendoza, J. A., De La Cruz-Soto, J., and Martínez-García, M. (2020). Fault estimation and fault tolerant control strategies applied to VTOL aerial vehicles with soft and aggressive actuator faults. *IEEE Access*, 8:10649–10661.

Ortiz-Torres, G., Castillo, P., Sorcia-Vázquez, F. D. J., Rumbo-Morales, J. Y., Brizuela-Mendoza, J. A., De La Cruz-Soto, J., and Martínez-García, M. (2020a). Fault estimation and fault tolerant control strategies applied to VTOL aerial vehicles with soft and aggressive actuator faults. *IEEE Access*, 8:10649–10661.

Ortiz-Torres, G., Castillo, P., Sorcia-Vázquez, F. D. J., Rumbo-Morales, J. Y., Brizuela-Mendoza, J. A., De La Cruz-Soto, J., and Martínez-García, M. (2020b). Fault estimation and fault tolerant control strategies applied to vtol aerial vehicles with soft and aggressive actuator faults. *IEEE Access*, 8:10649–10661.

Outeiro, P., Cardeira, C., and Oliveira, P. (2021). Multiple-model control architecture for a quadrotor with constant unknown mass and inertia. *Mechatronics*, 73:102455.

Poultney, A., Kennedy, C., Clayton, G., and Ashrafiuon, H. (2018). Robust tracking control of quadrotors based on differential flatness: Simulations and experiments. *IEEE/ASME Transactions on Mechatronics*, 23(3):1126–1137.

Qian, L. and Liu, H. H. (2019). Path-following control of a quadrotor uav with a cable-suspended payload under wind disturbances. *IEEE Transactions on Industrial Electronics*, 67(3):2021–2029.

Sadeghzadeh, I., Mehta, A., Chamseddine, A., and Zhang, Y. (2012). Active fault tolerant control of a quadrotor uav based on gainscheduled PID control. In *2012 25th IEEE Canadian Conference on Electrical and Computer Engineering (CCECE)*, pages 1–4. IEEE.

Saeed, A. S., Younes, A. B., Islam, S., Dias, J., Seneviratne, L., and Cai, G. (2015). A review on the platform design, dynamic modeling and control of hybrid UAVs. In *2015 International Conference on Unmanned Aircraft Systems (ICUAS)*, pages 806–815. IEEE.

Safaeipour, H., Forouzanfar, M., and Casavola, A. (2021). A survey and classification of incipient fault diagnosis approaches. *Journal of Process Control*, 97:1–16.

Sanz, R., Garcia, P., Zhong, Q.-C., and Albertos, P. (2016). Robust control of quadrotors based on an uncertainty and disturbance estimator. *Journal of Dynamic Systems, Measurement, and Control*, 138(7).

Sanz, R., García, P., Zhong, Q.-C., and Albertos, P. (2017). Predictor-based control of a class of time-delay systems and its application to quadrotors. *IEEE Transactions on Industrial Electronics*, 64(1):459–469.

Sariyildiz, E., Oboe, R., and Ohnishi, K. (2019). Disturbance observer-based robust control and its applications: 35th anniversary overview. *IEEE Transactions on Industrial Electronics*, 67(3):2042–2053.

Schacht-Rodríguez, R., P. J. G.-B. C. (2018). Path planning generation algorithm for a class of uav multirotor based on state of health of lithium polymer battery. *J Intell Robot Syst*, 91:115–131.

Silva, A. L. and Santos, D. A. (2020). Fast nonsingular terminal sliding mode flight control for multirotor aerial vehicles. *IEEE Transactions on Aerospace and Electronic Systems*, 56(6):4288–4299.

Yin, S., Xiao, B., Ding, S. X., and Zhou, D. (2016). A review on recent development of spacecraft attitude fault tolerant control system. *IEEE Transactions on Industrial Electronics*, 63(5):3311–3320.

Yu, Z., Qu, Y., and Zhang, Y. (2019). Fault-tolerant containment control of multiple unmanned aerial vehicles based on distributed sliding-mode observer. *Journal of Intelligent & Robotic Systems*, 93(1-2):163–177.

Zhang, Y. and Jiang, J. (2008). Bibliographical review on reconfigurable fault-tolerant control systems. *Annual reviews in control*, 32(2):229–252.

Zhong, Q.-C. and Rees, D. (2004). Control of uncertain lti systems based on an uncertainty and disturbance estimator. *Journal of Dynamic Systems, Measurement, and Control(Transactions of the ASME)*, 126(4):905–910.

Zulu, A. and John, S. (2016). A review of control algorithms for autonomous quadrotors. *arXiv preprint arXiv:1602.02622*.